Annals of 3D Printed Medicine 23 (2026) 100237

Contents lists available at ScienceDirect

Annals of 3D Printed Medicine

journal homepage: www.elsevier.com/locate/stlm

Research paper

Impact of MRI integration in CT-based planning on the accuracy of patient-specific 3D-printed shelf implant placement: a comparative cadaveric study

Milou FT Hüsken [a,b,*], Joëll Magré [a,c], Koen Willemsen [a], Harrie Weinans [a,d], Jafar Nasrabadi [a,e], Mahdi Bazargan [a,e], Vahid Arbabi [a,f], Alexander Meynen [f], Rintje Agricola [g,h], Björn Meij [i], Ralph Sakkers [a], Joris Bekkers [b], Bart CH vander Wal [a,j]

[a] Department of Orthopedics, University Medical Center Utrecht, Utrecht, the Netherlands
[b] Clinical Orthopedic Research Centre (CORC-mN), Diakonessenhuis, Utrecht, Zeist, the Netherlands
[c] 3D lab, Division of surgical specialties, University Medical Center Utrecht, Utrecht, the Netherlands
[d] Department Biomechanical Engineering, 3ME, TU Delft, Delft, the Netherlands
[e] Department of Mechanical Engineering, Faculty of Engineering, University of Birjand, Birjand, Iran
[f] Replasia BV, Leuven, Belgium
[g] Department of Orthopedics and Sports medicine, Erasmus University Medical Center, Rotterdam, the Netherlands
[h] Department of Orthopedics, Anna Hospital, Geldrop, the Netherlands
[i] Department of Clinical Sciences, Faculty of Veterinary Medicine, Utrecht University, Utrecht, the Netherlands
[j] Department of Orthopedics, Leiden University Medical Center, Leiden, the Netherlands

ARTICLE INFO

Keywords:
3D printing
Patient-specific implant
Hip dysplasia
Shelf arthroplasty
MRI
CT planning
Cadaver study

ABSTRACT

Introduction: Hip dysplasia, characterized by an insufficient acetabular coverage of the femoral head, increases hip joint stress and predisposes to degenerative changes. A novel 3D-printed, patient-specific extracapsular shelf implant was developed to increase femoral head coverage. Accurate implant placement is crucial. This cadaveric study compared CT-only surgical planning with combined CT- and MRI-based planning to evaluate whether MRI integration improves positioning accuracy.

Methods: Two cohorts of non-dysplastic cadaveric hips were studied. In cohort 1 (five hips), implant design was based solely on CT imaging. In cohort 2 (four hips), both CT and MRI datasets were used, incorporating capsular soft-tissue anatomy. Postoperative implant positioning was compared with preoperative plans using point-cloud analyses, clockface coverage graphs, and Dice coefficients. Acceptable placement was defined as: median Euclidean distance < 5 mm, median angular deviation $< 5°$, and Dice > 0.75 respectively.

Results: In the CT-only cohort, three of five implants failed one or more accuracy thresholds, with Euclidean distances up to 8.5 mm, coverage deviations up to 6°, and Dice coefficients as low as 0.37. CT-only designed implants consistently tilted away from the acetabular rim, reflecting underestimation of hip capsule thickness and insertion height. In the CT+MRI cohort, all four implants met the <5 mm and <5° deviation thresholds, and three achieved Dice ≥ 0.75. No consistent deviation patterns were observed.

Conclusion: Combined CT and MRI planning improved implant positioning accuracy by better accounting for variations in hip capsule morphology. MRI integration demonstrated superior performance over CT-only planning for patient-specific shelf implant placement.

Introduction

In patients with hip dysplasia, the acetabulum is typically shallower and more anteverted, while the femoral head tends to be more elliptical in shape [1], resulting in insufficient femoral head coverage, reduced joint contact, and increased mechanical stress on the hip, labrum, and

Abbreviations: APP, Anterior pelvic plane; CT, Computed tomography; CT+MRI, Combined computed tomography and magnetic resonance imaging; IQR, Interquartile range; LCEA, Lateral center-edge angle; MRI, Magnetic resonance imaging; PAO, Periacetabular osteotomy; SD, Standard deviation.

* Corresponding author at: postnumber L 01.629, Postbus 85500 3508 GA Utrecht, the Netherlands.
E-mail address: m.f.t.husken-3@umcutrecht.nl (M.F. Hüsken).

https://doi.org/10.1016/j.stlm.2026.100237
Received 21 April 2026; Accepted 28 April 2026
Available online 22 May 2026

hip capsule. Adult or residual hip dysplasia is radiographically defined by a Wiberg center-edge angle [2] below 20° and/or insufficient anterior or posterior acetabular walls, indicating inadequate femoral head coverage. Clinical symptoms may include groin pain, abnormal gait, reduced strength, and increased risk of degenerative hip disease [3].

Radiographic signs of dysplasia occur in 3.6–12.8% of the population, although not always with clinical symptoms [4,5]. In symptomatic patients, treatment aims to restore sufficient femoral head coverage to reduce joint stress. The commonly used surgical intervention is the periacetabular osteotomy (PAO), which reorients the acetabulum via multiple pelvic osteotomies followed by refixation [6,7]. Despite its efficacy, PAO is technically demanding and involves lengthy rehabilitation. Complication rates up to 37% have been reported, including residual dysplasia, overcorrection, and non-union [7] .

Shelf arthroplasty is an older technique in which autologous bone from the iliac crest is placed above the joint capsule [8,9], improving femoral head coverage and allowing the interposed capsule to act as a load-bearing surface. Complication rates are lower than in PAO, but accurate graft placement is also technically challenging. Inaccurate positioning may lead to insufficient load bearing or impingement. In a systematic review, Willemsen et al [9] noted that with accurate placement and proper patient selection (e. g., without advanced osteoarthritis or labral tears), the survival rates are comparable to PAO.

Dogs show hip dysplasia anatomically and clinically comparable to that in humans [10,11]. Our group developed a 3D-printed shelf implant for dogs with clinical hip dysplasia to improve coverage not only superior of the femoral head, but across the whole load-bearing surface [12–14]. These patient-specific 3D-printed shelf implants demonstrated adequate mechanical properties [12] and good short-term [13,15] and one-year clinical results in a cohort of dog patients with hip dysplasia [16].

Encouraged by these outcomes, a patient-specific 3D-printed shelf implant was developed for humans with hip dysplasia. This study focuses on the surgical feasibility and positioning accuracy of this implant in a controlled experimental setting. The main research question was whether CT imaging alone is sufficient for personalized 3D implant design based on bony anatomy, or if additional MRI data are required to capture soft-tissue structures of the hip for integration into the design process. Therefore, this cadaveric study evaluated whether incorporating MRI-derived information on hip capsule morphology into preoperative planning improves the positioning accuracy of a patient-specific 3D-printed shelf implant compared with CT-only planning.

Methods

Specimen and studydesign

CT scans and MRI scans were made of 9 non-dysplastic hips from 5 pelves. Implant design and preoperative planning were based solely on CT imaging in 5 hips from 3 pelves (cohort 1), where MRI was used for retrospective soft tissue evaluation. In 4 hips from 2 pelves (cohort 2), both CT and MRI datasets were used for implant design, allowing incorporation of soft tissue anatomy (hip joint capsule) in the design. The primary outcome was the agreement between planned and achieved implant position, quantified by the median Euclidean distance between surface point clouds, differences in acetabular coverage derived from clockface graphs, and Dice similarity coefficients.

Imaging

Pelvic CT scans with 0.9 mm slice thickness of the pelvis were obtained for preoperative planning and design of the implant and drill guide for each hip. MRI scans were performed using a 3T scanner (Ingenia; Philips Healthcare) with a torso coil and multi-echo gradient-echo sequence. Axial images were acquired at 1.2 × 1.2 × 2 mm and reconstructed to 0.97 × 0.97 × 1 mm resolution.

Preoperative implant design

CT scans were segmented in Mimics (v24; Materialise, Leuven, Belgium) using bone thresholding and manual correction to generate 3D models. The pelves were aligned to the 0-degree anterior pelvic plane (APP) for sagittal alignment, and coronal rotation was neutralized by aligning acetabular centers of rotation. A radial coverage clock-face graph as described by Larson et al [17], was generated for each pelvis. For dysplastic hips, patient-specific shelf implants are intended to increase acetabular rim coverage to at least 25° lateral center-edge angle (LCEA); for the non-dysplastic cadaveric hips in this study, implants were designed to increase the native (already sufficient) coverage by an additional 15° LCEA.

In cohort 1 (CT-only design), the implant was based solely on CT-derived bone morphology; soft-tissue thickness and capsule insertion height were approximated using values from existing literature [18], applying a uniform offset of 5 mm width and 10 mm height for the hip capsule interposition and allow for a slight compression. In cohort 2 (CT + MRI design), both CT and MRI datasets were used, and the actual soft-tissue thickness and capsule insertion height were measured individually on the MRI scan.

Implant design was performed in Geomagic Freeform (Version 2022.0.34; 3D Systems, South Carolina, USA). Implant and drill guide were 3D-printed by powder-bed fusion in medical-grade titanium (Ti-6Al-4 V ELI Grade 23) by Amnovis, Aarschot, Belgium (Fig. 1). The drill guide contained five predefined holes: two drill holes for 6 mm pegs, one drill hole for a 3.2 mm non-locking screw and two holes for temporary fixation of the drill guide with 2.0 mm k-wires. The implant was designed with two pegs to aid accurate positioning and to distribute load and was fixed with one non locking cortical screw to create lag compression, plus 3 locking screws for angle stable fixation. The screw trajectories were planned with divergent angles to allow secure fixation within the ilium while remaining reachable through the anterior approach.

Surgical procedure

An anterior approach to the hip was used with the patient in the supine position. A 10 cm incision, slightly more cranial than the conventional anterior approach, was made to access the ilium. Soft tissue over the iliac crest and hip capsule was cleared to allow placement of the drill guide in direct contact with bone without opening the joint capsule; if necessary, the capsule insertion was slightly peeled distally to improve fit. The 3D-printed shelf implant was positioned using the patient-specific titanium drill guide.

After optimal guide positioning under fluoroscopy, the guide was fixed with two 2.0 mm K-wires. The peg holes were drilled with a 6 mm drill bit with pre-measured depth and a drill stop to avoid bicortical perforation, followed by drilling of the non-locking screw hole with a 3.2 mm drill. After removing the guide, the implant was inserted using the pre-drilled peg holes and pulled to the bone with a 4.5 mm non-locking self-tapping cortical screw. Final fixation was achieved with three bicortical 5.0 mm self-tapping locking Ti-6Al-7Nb screws with hex drive, after predrilling with 4.3 mm drills (DePuy Synthes, Zuchwil, Switzerland). Screw lengths were pre-measured and verified with a depth gauge before insertion.

Outcome measures

Postoperative CT images were segmented and aligned with the preoperative CT scan images to quantify positional deviations. The accuracy of each implant was evaluated using the Euclidean distance between corresponding surface points, the difference in acetabular rim coverage derived from clockface graphs, and the Dice similarity

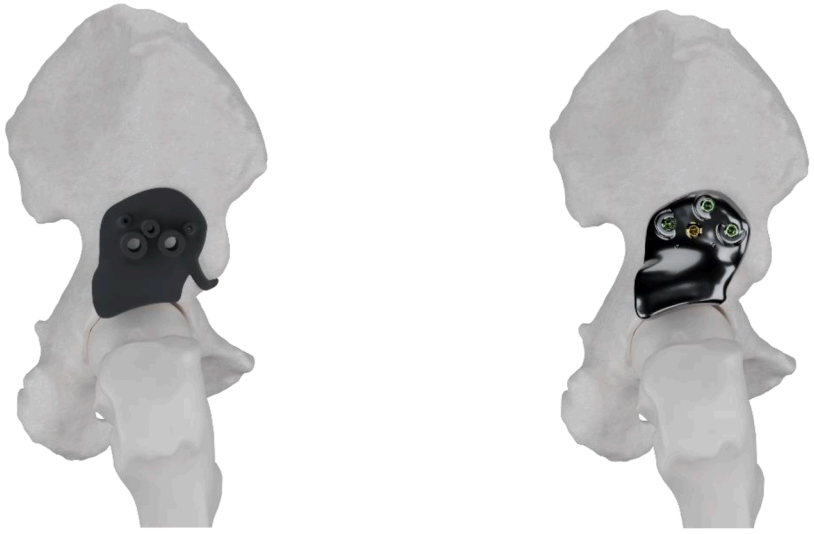

Fig. 1. Illustrative design example of the drill guide (left) and the 3D shelf implant (right) with the planned position in accordance to the femoral head with space for the hip capsule in a dysplastic hip joint.

coefficient representing volumetric overlap between planned and achieved implant positions. To calculate Euclidean distances, all implant surfaces were re-meshed with uniform 0.2 mm edge lengths, generating evenly distributed point clouds and minimizing potential bias due to non-uniform mesh density (Fig. 2). For each specimen the minimal, maximal (Hausdorff), and median Euclidean distances were recorded in mm together with interquartile ranges. Differences in degrees acetabular rim coverage between the preoperative plan and postoperative positioning were quantified in degrees using the clockface method described by Larson et al [17]. The Dice coefficient was used to assess volumetric overlap, with values ranging from 0 (no overlap) to 1 (complete correspondence).

Optimal placement was defined as zero deviation in Euclidean distance and coverage graphs, with a Dice coefficient of 1. Placement was considered acceptable when the median Euclidean distance was below 5 mm, the median coverage difference below 5°, and the Dice coefficient above 0.75. These thresholds were pragmatically defined for this exploratory technical study, as validated cut-off values for this novel implant are not yet available, but were chosen to reflect deviations that could plausibly result in clinically relevant under- or overcorrection in future applications.

The outcomes of these analyses, including assessment against the predefined criteria for acceptable placement, were compared between cohort 1 (implant design based solely on CT) and cohort 2 (implant design incorporating both CT and MRI datasets).

Results

Surgical procedures

The surgeries were performed by the 2 different surgeons, the first by JB and second by RA, both extensive experience in hip surgery but limited experience with this novel extra capsular implant. Patient-specific drill guides, shelf implants, and screws were successfully placed using the direct anterior hip approach. The hip capsule insertion was slightly peeled downwards in cohort 1 for implants 2, 3, and 5 to improve guide and implant fit; this maneuver was not required in cohort 2.

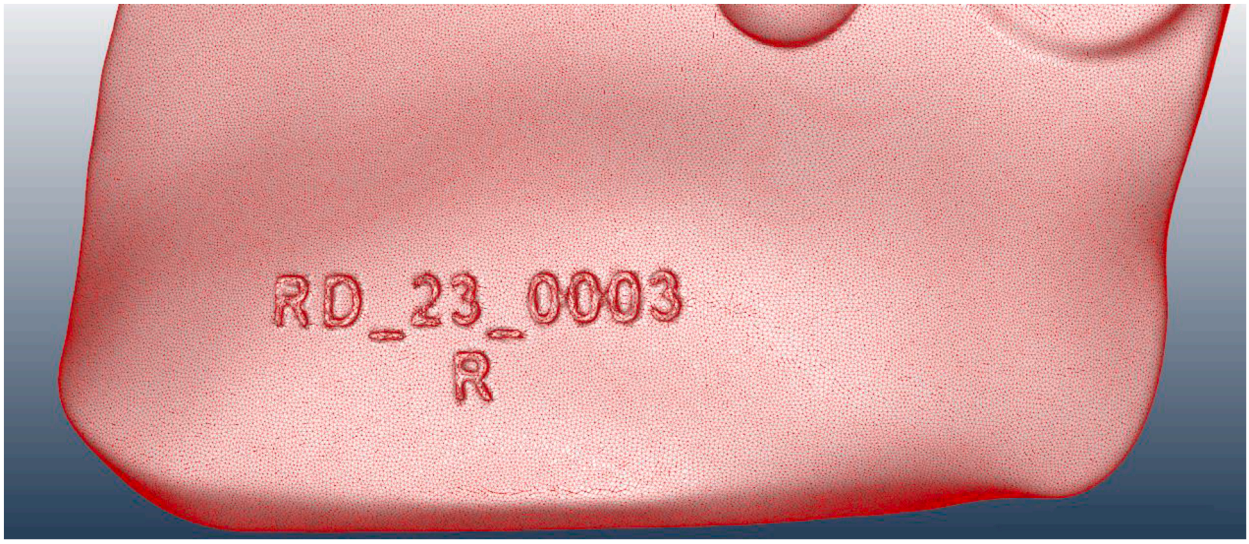

Fig. 2. Example of a point cloud generated on the segmented surface of the 3D shelf implant.

Cohort 1: CT-only -Based planning

The median Euclidean distance ranged from 1.69 mm (IQR 1.58–1.82) for implant number 1 to 8.49 mm (IQR 6.66–9.92) for implant number 5. Only implant number 5 exceeded the predefined acceptable median deviation of 5 mm (median 8.49 mm). Table 1 summarizes the minimal, maximal, mean (SD), and median (IQR) Euclidean distances, coverage differences, and Dice coefficients for each implant compared to the preoperative plan.

Clockface graphs demonstrated alignment between planned and postoperative positions, with median angular deviations of 2–6° (Table 1). Implants 4 and 5 exceeded the predefined acceptable limit of 5° (both 6°).

The Dice coefficient, quantifying volumetric overlap between planned and achieved implant placement, ranged from 0.37 to 0.92. The threshold of 0.75 was not reached for implants 2, 4, and 5 (0.71, 0.37, and 0.74, respectively). The implants showed a lateral tilt away from the rim, particularly for implants 4 and 5, but to a lesser extent also for implant 2 (Fig. 3). The narrow interquartile range (IQR) suggests that the entire implant shifted uniformly in a specific direction, indicating a translational movement rather than a rotational misalignment, which would typically result in a wider range of point-to-point distances.

The preoperative MRI scans were hereafter used to find possible explanations for the unacceptable placements of implants 2, 4 and 5. This revealed intersection between the implant and the hip capsule, most prominently for implants 4 and 5 (Fig. 4) In all implants of cohort 1, the actual capsule insertion height exceeded the assumed 10 mm For implants 1 and 4, insertion heights up to 15 mm caused positional impact with deviations <5 mm. Differences larger than 15 mm were observed for implants 2, 4 and 5, with 17.5, 15.6 and 17.4 mm respectively, causing larger deviations (Table 2). Capsule thickness was greatest for implants 4 and 5 (respectively 14.0 and 13.7 mm) clearly exceeding the 5 mm assumption, whereas smaller deviations for implants 1, 2, and 3 (<1 mm) had negligible effects on implant positioning.

Cohort 2: CT ± MRI-Based planning

In cohort 2, implant design incorporated both CT and MRI data, using direct measurement data of capsule thickness and insertion height for each specimen. The insertion height and capsules thickness were measured using theMRI data and used as design offsets (Table 3). The minimal, maximal, mean (SD), and median (IQR) Euclidean distances, coverage differences, and Dice coefficients for each implant compared to the preoperative plan (Table 4). The median Euclidean distance ranged from 0.91 mm (IQR 0.80–1.04) for implant number 4 to 2.83 mm (IQR 2.34–3.74) for implant number 1. All implants in cohort 2 were placed within the acceptable 5 mm median deviation.

Differences in clockface graphs in cohort 2 between planned and postoperative positions were minimal, with median deviations between 0.5° and 4.5° Two implants showed a maximum deviation of 8.5° (implant 2) and 7.5° (implant 3), though the median remained well within acceptable limits.

The Dice coefficients in cohort 2 demonstrated high volumetric overlap. The cutoff Dice coefficient of 0.75 was not reached for implant 1 (0.56) and when observing the postoperative placement for implant 1 (Fig. 5), there appeared to be a slight cranial placement with mainly some detachment from the underlying bone. However, the median displacement and clockface graph stayed within the predefined limits, which indicated an adequate implant positioning overall. No systematic deviations were observed in cohort 2, and interquartile ranges were consistently narrow, confirming stable and reproducible placement across specimens.

Cohort comparison

Three out of five cohort 1 implants failed one or more predefined accuracy thresholds due to unaccounted capsule variability (thickness up to 14.0 mm, insertion height up to 17.5 mm), causing systematic tilting away from the acetabular rim. All cohort 2 implants met Euclidean distance and angular deviation thresholds, three out of four also met the overlap threshold. Incorporating patient-specific MRI data eliminated systematic deviation patterns observed in CT-only planning.

Discussion

In this study the positioning accuracy of the extracapsular 3D shelf implant was evaluated using planning on CT data only and planning on both CT and MRI data. The incorporation of soft tissue data by using combined CT and MRI data was superior in the design and positioning accuracy of patient-specific 3D-printed shelf implants over the use of CT data only.

Cohort 1 analysis demonstrated that CT-only planning, using fixed assumptions of 5 mm capsule thickness and 10 mm insertion height, resulted in consistent deviations from planned implant positioning. Only implants 1 and 3 met predefined criteria, though implant 3 bordered the Euclidean threshold. Implants 2, 4, and 5 exceeded acceptable limits primarily due to thicker capsules (>10 mm) and higher insertion points (>17 mm) than assumed. For implants 4 and 5, capsule thickness reached 14.0 and 13.7 mm respectively, which caused the implant to rest on top of the hip capsule rather than integrating with bone, causing tilting of the implant. Capsule insertion discrepancies >15 mm (up to 17.5 mm) in implants 2, 4, and 5 further compromised positioning accuracy.

These findings demonstrate that CT-only planning is insufficient for

Table 1
Cohort 1 - Difference between digital planning and postoperative position during the cadaveric tests in absolute (Euclidean) distance and coverage (degrees).

	Euclidean Distance (mm)					Coverage Difference (°)					Dice score coefficient
	Min distance	Max distance (Hausdorff)	Median	IQR		Min difference	Max difference	Median difference rim implant	IQR		
				25%	75%				25%	75%	
IMPLANT NO. 1	1.42	2.27	1.69	1.58	1.82	2	7	3	2.5	4	0.92
IMPLANT NO. 2	2.11	4.01	2.79	2.41	3.25	3	8	4	4	5	**0.71**
IMPLANT NO. 3	2.82	6.48	4.50	3.85	5.44	1	5	2	1	3	0.82
IMPLANT NO. 4	2.97	4.70	3.79	3.43	4.20	5	10	**6**	6	7	**0.37**
IMPLANT NO. 5	3.32	11.81	**8.49**	6.66	9.92	5	12	**6**	5	7	**0.74**

Euclidean Distance = absolute distance between planned position and reached position in millimeters (mm), Coverage Difference = Difference in coverage between planned position and reached position in degrees (°), Dice score calculated by 2 × intersection volume/volume object A + volume object B. Min = minimal, Max = maximal, IQR = Interquartile range,.

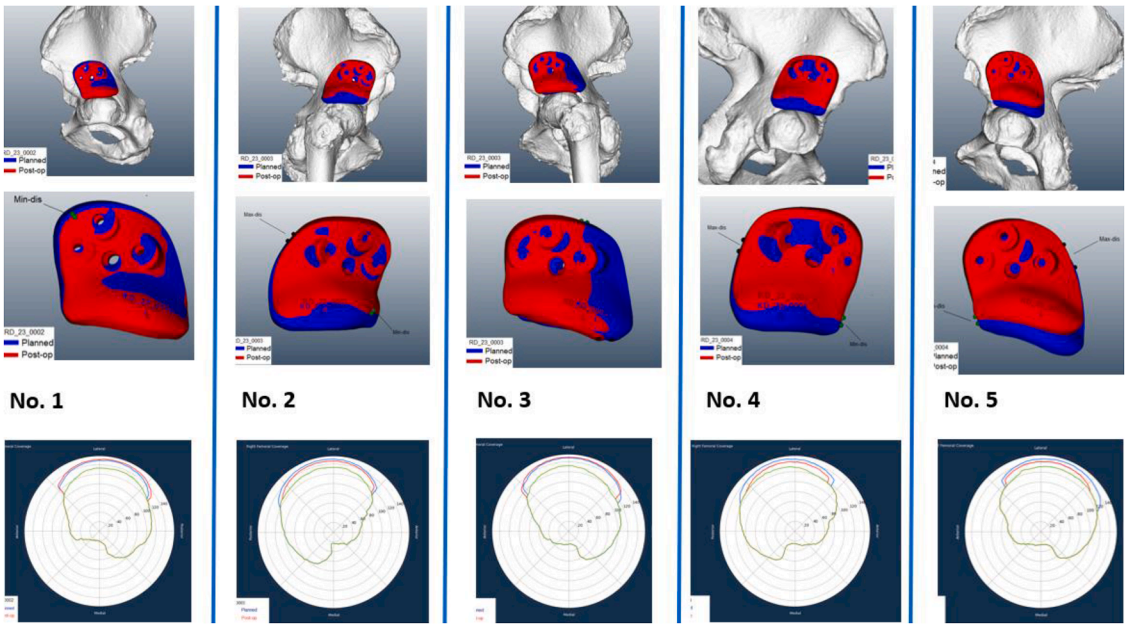

Fig. 3. Cohort 1. Above: placement of the 3D-printed shelf Implant; blue is planned position, red is postoperative position. Below: Clockface graphs of the 3D-printed shelf implant; blue is planned position, red is postoperative position, green is original acetabulum of the healthy cadaveric specimen.

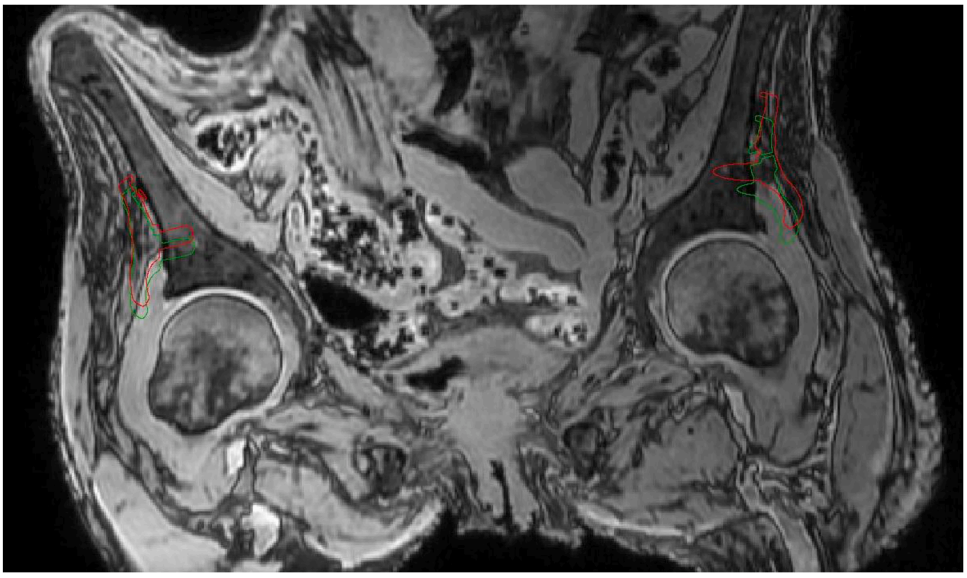

Fig. 4. MRI of the pelvis cadaver number 3, in cohort 1 for implants 4 (left) and 5 (right), showing a more cranial position of the implant due to the enlarged hip capsule. Green is the planned position, red is the postoperative position.

patient-specific shelf implant design because fixed soft-tissue assumptions fail to account for anatomical variability. Intraoperative capsule peeling mitigated some discrepancies but introduced procedural variability unsuitable for reproducible clinical application. Cohort 2 confirmed that incorporating patient-specific MRI measurements of capsule thickness and insertion height yielded superior positioning accuracy. Although the sample size is small, median Euclidean distances were more than halved, coverage deviations decreased to below 5°, and most Dice coefficients exceeded 0.75. These findings indicate that MRI enhances the implant design by accurately incorporating patient-specific soft tissue dimensions, improving correspondence between the planned and achieved implant positions.

Hip capsule morphology

Variability in hip capsule morphology poses a major challenge in the placement of the shelf in extracapsular surgery for hip dysplasia. Some studies report reduced thickness and delamination of the hip capsule in patients with hip dysplasia [19,20], while others describe thickening associated with hypermobility or periarthritis [21,22]. More recent findings indicate that both thinning (instability) and thickening (adaptive stress response) may occur [23]. The degree in variations in capsule thickness indicates that the use of an estimated thickness in planning is likely to be inadequate and results in deviated implant positioning from planning.

Table 2
Difference between digital CT-only planning in cohort 1 and measured hip capsule thickness and hip capsule insertion height on MRI. The differences in the (assumed) offset height (left), width (middle) and a summary of the positioning results (right) are shown.

	Hip capsule insertion height/ Offset height (mm)			Hip capsule thickness / Offset width (mm)			Summary results positioning versus planning		
	Insert height used for design	Remeasured	Discrepancy	Offset width used for design	Remeasured	Discrepancy offset and hip capsule	Median Euclidean distance	Median Coverage difference	Dice score
IMPLANT NO. 1	10	11.6	1.6	5	5.6	0.6	1.69	3	0.92
IMPLANT NO. 2	10	17.5	**7.5** *	5	5.5	0.5	2.79	4	**0.71** *
IMPLANT NO. 3	10	15.6	5.6	5	5.4	0.4	4.50	2	0.82
IMPLANT NO. 4	10	14.2	4.2	5	14.0	**9.0** *	3.79	**6** *	**0.37** *
IMPLANT NO. 5	10	17.4	**7.4** *	5	13.7	**13.7** *	**8.49** *	**6** *	**0.74** *

Euclidean Distance = absolute distance between planned position and reached position in millimeters (mm), Coverage Difference = Difference in coverage between planned position and reached position in degrees (°), Dice score calculated by 2 × intersection volume/volume object A + volume object B. Remarkable big deviations are indicated by asterisk (*).

Table 3
Measured hip capsule thickness and hip capsule insertion height on MRI for cohort 2. The offset height (left), an hip capsule thickness (middle) are directly used into the implant design. A summary of the positioning results (right) are shown.

	Hip capsule insertion height/ Offset height (mm)			Hip capsule thickness / Offset width (mm)	Summary results positioning versus planning		
	Anterior	Mid	Posterior	Offset width	Median Euclidean distance	Median Coverage difference	Dice score
IMPLANT NO. 1	19	14.5	14.9	6	2.83	0.5	**0.56** *
IMPLANT NO. 2	18	18	18	6	2.55	4.5	0.75
IMPLANT NO. 3	14	14	8	8.5	1.56	2.5	0.76
IMPLANT NO. 4	14.5	14	9	7	0.91	0.5	0.86

Measurements are shown in millimeters (mm), Euclidean Distance = absolute distance between planned position and reached position in millimeters (mm), Coverage Difference = Difference in coverage between planned position and reached position in degrees (°), Dice score calculated by 2 × intersection volume/volume object A + volume object B. Remarkable big deviations are indicated by asterisk (*).

Table 4
Cohort 2 - Difference between digital planning and postoperative reached position during the cadaveric tests in absolute (Euclidean) distance and coverage (degrees).

	Euclidean Distance (mm)					Coverage difference (°)					Dice score coefficient
	Min distance	Max distance (Hausdorff)	Median distance	IQR		Min difference	Max difference	Median difference rim implant	IQR		
				25%	75%				25%	75%	
IMPLANT NO. 1	1.28	5.06	2.83	2.34	3.74	0	4.5	0.5	0.5	0.5	0.56
IMPLANT NO. 2	0.85	4.30	2.55	1.92	3.17	2	8.5	4.5	4.5	5	0.75
IMPLANT NO. 3	1.03	3.73	1.56	1.26	2.07	1.5	7.5	2.5	2	3	0.76
IMPLANT NO. 4	0.69	1.23	0.91	0.80	1.04	0	1.5	0.5	0	0.5	0.86

Euclidean Distance = absolute distance between planned position and reached position in millimeters (mm), Coverage Difference = Difference in coverage between planned position and reached position in degrees (°), Dice score calculated by 2 × intersection volume/volume object A + volume object B. Min = minimal, Max = maximal, IQR = Interquartile range.

Remaining displacement

The suboptimal placed implants tended to tilt away from the acetabular rim, which can be explained by the underlying hip capsule which is not accounted for in planning. A tilt toward the joint risks impingement or cartilage damage due to locally increased stresses, whereas lateral displacement primarily compromises femoral coverage. It is worth noting that, despite relatively large positional deviations and low Dice scores, the median femoral head coverage is not always markedly affected.

In studies in dogs by Willemsen et al [12,13 ,15], slightly inaccurate positioning of the implants was followed by soft-tissue adaptation such as capsule hypertrophy that filled the space between implant and capsule without necrosis [13]. These findings suggest that minor misplacements may also be compensated for by soft tissue remodeling in humans, and that the surgery might by clinically successful even when the implant has not been positioned optimally from a radiological standpoint, although this must be confirmed in future clinical studies.

Methodological considerations

A potential influence of a surgical learning curve should be considered. Although cohort 2 was performed after cohort 1, the procedures were carried out by different surgeons (JB for cohort 1 and RA for cohort

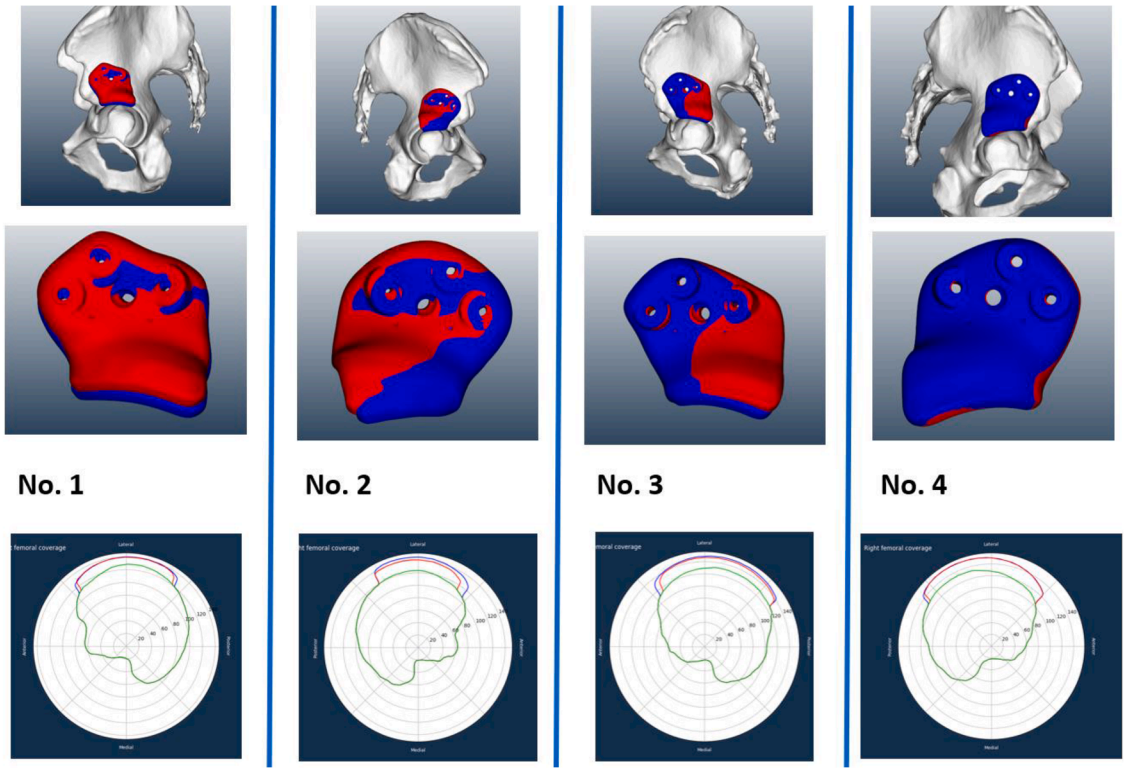

Fig. 5. Cohort 2. Above: placement of the 3D-printed shelf Implant; blue is planned position, red is postoperative position. Below: Clockface graphs of the 3D-printed shelf implant; blue is planned position, red is postoperative position, green is original acetabulum of the healthy cadaveric specimen.

2). Both surgeons had completed a prior cadaver training session on the same surgical technique, suggesting a comparable baseline level of familiarity with the approach and instrumentation. Deviations observed in cohort 1 were consistent in direction and related to soft-tissue interposition rather than inconsistent handling, whereas cohort 2 showed no uniform displacement pattern. These findings imply that the improved accuracy observed in cohort 2 is more likely attributable to enhanced preoperative planning through MRI integration than to procedural learning alone, although a residual learning effect cannot be entirely excluded.

The use of non-dysplastic cadaveric hips limits the applicability of these findings to clinical populations with developmental dysplasia. Dysplastic hips typically exhibit greater anatomical variability, including altered acetabular morphology and soft tissue adaptations such as changes in capsule thickness, which could further influence implant positioning accuracy. Conversely, such variability might enhance the fit of a patient-specific guide and implant as the unique bone morphology could improve mechanical interlocking.

Future perspective

This study highlights the importance of individualized preoperative planning and combining imaging to account for soft tissue variability when designing extra-capsular, patient-specific shelf implants. Incorporating CT and MRI data allows for accurate characterization of bone and soft tissue, reducing the need for intraoperative adjustments such as capsule peeling and improving consistency of results.

As no validated or predetermined cut-off values exist for acceptable positioning of the 3D-printed shelf implant, the thresholds used in this study were defined pragmatically based on anticipated clinical relevance. Similar to periacetabular osteotomies (PAO), target values for acceptable positioning should be established through clinical outcome studies rather than predefined intraoperative cut-offs. For the implant used in our study, such clinical outcome data are not yet available and could be re-evaluated in the future.

Conclusion

Combined CT and MRI planning improved implant positioning accuracy by better accounting for variations in hip capsule morphology. MRI integration in CT design demonstrated superior performance over CT-only planning for patient-specific shelf implant placement.

Author contributions

Conceptualization and methodology were developed by MH, JM, KW, HW, RS, JB, and BvdW. Implant designs and adaptations were contributed by JM, KW, JN, MB, VA, AM, HW, RS, JB, and BvdW. Surgeries were performed by JB and RA. JM segmented the CT scans; MH, JM, and JN performed the formal data analysis. The original draft, including figures and charts, was written by MH and JM, with all authors involved in reviewing and editing the manuscript. Project supervision was provided by HW, RS, JB, and BvdW. All authors approved the final manuscript.

Funding

This research was financially supported by the PRosPERoS-II project, funded through the Interreg VA Flanders–the Netherlands program, CCI grant no. 2021TC16RFCB041.

Ethics approval and consent to participate

Formal Medical Research Ethics Committee approval was not required for this study because no living participants were involved and all specimens had been donated for scientific and educational use under the institutional body donation program. All procedures were conducted in accordance with institutional regulations and applicable national

legislation governing the use of donated human bodies. Donor privacy and confidentiality were protected throughout the study.

Data availability

The data that support the findings of this study are available from the corresponding author upon reasonable request.

Declaration of competing interest

Milou F. T. Hüsken and Vahid Arbabi were employed by Replasia B. V. during parts of this study. Alexander Meynen is employed by Replasia B.V. still. Harrie Weinans has received various research grants and holds minority shares in Replasia BV, Uplanner BV, and Amotio BV, and has patents pending in related areas. Ralph J. B. Sakkers is listed as inventor on multiple orthopedic implant patents and holds shares in UPlanner BV and Replasia BV. He also serves in leadership roles in the European Paediatric Orthopaedic Society and the Osteogenesis Imperfecta Federation Europe, among others. Bart C. H. van der Wal holds patents related to orthopedic implants, has minority shares in Replasia BV, Amotio BV, and Uplanner BV, and serves on advisory boards for these companies. The other authors declare no competing interests.

References

[1] Zhang M, Liu BL, Qi XZ, Yang QQ, Sun JY, Zheng QY, Zhang GQ, Cheng CK. The three-dimensional morphology of femoral medullary cavity in the developmental dysplasia of the hip. Front Bioeng Biotechnol 2021;9:684832. https://doi.org/10.3389/fbioe.2021.684832.

[2] Wiberg G. Studies on dysplastic acetabula and congenital subluxation of the hip joint with special reference to the complication of osteoarthritis. Acta Chir Scand 1939:5–135.

[3] Gala L, Clohisy JC, Beaule PE. Hip dysplasia in the young adult. J Bone Jt Surg Am 2016;98(1):63–73. https://doi.org/10.2106/JBJS.O.00109.

[4] Gosvig KK, Jacobsen S, Sonne-Holm S, Palm H, Troelsen A. Prevalence of malformations of the hip joint and their relationship to sex, groin pain, and risk of osteoarthritis: a population-based survey. J Bone Jt Surg Am 2010;92(5):1162–9. https://doi.org/10.2106/JBJS.H.01674.

[5] Jacobsen S, Sonne-Holm S. Hip dysplasia: a significant risk factor for the development of hip osteoarthritis. A cross-sectional survey. Rheumatology 2005;44(2):211–8. https://doi.org/10.1093/rheumtology/keh436. 2004/10/14.

[6] Ganz R, Klaue K, Vinh TS, Mast JW. A new periacetabular osteotomy for the treatment of hip dysplasias. Technique and preliminary results. Clin Orthop Relat Res 1988;232(232):26–36.

[7] Clohisy JC, Schutz AL, St John L, Schoenecker PL, Wright RW. Periacetabular osteotomy: a systematic literature review. Clin Orthop Relat Res 2009;467(8):2041–52. https://doi.org/10.1007/s11999-009-0842-6.

[8] König F. Osteoplastische behandlung der congenitalen hüftgelenkluxation. Verh Dtsch Ges Chir 1891;(20):75–80.

[9] Willemsen K, Doelman CJ, Sam ASY, Seevinck PR, Sakkers RJB, Weinans H, van Der Wal BCH. Long-term outcomes of the hip shelf arthroplasty in adolescents and adults with residual hip dysplasia: a systematic review. Acta Orthop 2020;91(4):383–9. https://doi.org/10.1080/17453674.2020.1747210.

[10] Pascual-Garrido C, Guilak F, Rai MF, Harris MD, Lopez MJ, Todhunter RJ, Clohisy JC. Canine hip dysplasia: a natural animal model for human developmental dysplasia of the hip. J Orthop Res 2018;36(7):1807–17. https://doi.org/10.1002/jor.23828. 2017/12/12.

[11] Willemsen K, Moring MM, Harlianto NI, Tryfonidou MA, van der Wal BCH, Weinans H, Meij BP, Sakkers RJB. Comparing hip dysplasia in dogs and humans: a review. Front Vet Sci 2021;8:791434. https://doi.org/10.3389/fvets.2021.791434. 2022/01/04.

[12] Willemsen K, Tryfonidou M, Sakkers R, Castelein RM, Zadpoor AA, Seevinck P, Weinans H, Meij B, van der Wal BCH. Patient-specific 3D-printed shelf implant for the treatment of hip dysplasia: anatomical and biomechanical outcomes in a canine model. J Orthop Res 2022;40(5):1154–62. https://doi.org/10.1002/jor.25133. 2021/07/01.

[13] Willemsen K, Tryfonidou MA, Sakkers RJB, Castelein RM, Beukers M, Seevinck PR, Weinans H, van der Wal BCH, Meij BP. Patient-specific 3D-printed shelf implant for the treatment of hip dysplasia tested in an experimental animal pilot in canines. Sci Rep 2022;12(1):3032. https://doi.org/10.1038/s41598-022-06989-9.

[14] Kwananocha I, Verseijden F, Kamali SA, Magre J, Willemsen K, Schouten JC, Salvatori D, Tryfonidou MA, Meij BP. Surgical technique of the 3-dimensional-printed personalized hip implant for the treatment of canine hip dysplasia. J Vis Exp 2024;(206). https://doi.org/10.3791/66005.

[15] Kwananocha I, Magre J, Willemsen K, Weinans H, Sakkers RJB, How T, Verseijden F, Tryfonidou MA, van der Wal BCH, Meij BP. Acetabular rim extension using a personalized titanium implant for treatment of hip dysplasia in dogs: short-term results. Front Vet Sci 2023;10:1160177. https://doi.org/10.3389/fvets.2023.1160177.

[16] Kwananocha I, Magre J, Kamali A, Verseijden F, Willemsen K, Ji Y, van der Wal BCH, Sakkers RJB, Tryfonidou MA, Meij BP. Outcome one year after acetabular rim extension using a customized titanium implant for treating hip dysplasia in dogs. Animals 2024;14(16):2385. https://doi.org/10.3390/ani14162385.

[17] Larson CM, Moreau-Gaudry A, Kelly BT, Byrd JW, Tonetti J, Lavallee S, Chabanas L, Barrier G, Bedi A. Are normal hips being labeled as pathologic? A CT-based method for defining normal acetabular coverage. Clin Orthop Relat Res 2015;473(4):1247–54. https://doi.org/10.1007/s11999-014-4055-2. 2014/11/20.

[18] Kay J, Memon M, Rubin S, Simunovic N, Nho SJ, Belzile EL, Ayeni OR. The dimensions of the hip capsule can be measured using magnetic resonance imaging and may have a role in arthroscopic planning. Knee Surg Sports Traumatol Arthoscopy 2020;28(4):1246–61. https://doi.org/10.1007/s00167-018-5162-5.

[19] Bai H, Fu YQ, Ayeni OR, Yin QF. The anterior hip capsule is thinner in dysplastic hips: a study comparing different young adult hip patients. Knee Surg Sports Traumatol Arthrosc 2023;31(1):70–8. https://doi.org/10.1007/s00167-022-07022-2. 2022/06/11.

[20] Metz AK, Lewis DC, Froerer DL, Featherall J, Rosenthal RM, Khalil AZ, Aoki SK. Dysplastic hips have decreased iliofemoral ligament thickness on coronal sequences in Magnetic resonance imaging: a matched cohort analysis. Arthroscopy 2025;41(4):992–9. https://doi.org/10.1016/j.arthro.2024.05.033.

[21] Devitt BM, Smith BN, Stapf R, Tacey M, O'Donnell JM. Generalized joint hypermobility is predictive of hip capsular thickness. Orthop J Sports Med 2017;5(4):2325967117701882. https://doi.org/10.1177/2325967117701882.

[22] Le Bouthillier A, Rakhra KS, Belzile EL, Foster RCB, Beaule PE. Soft tissue structures differ in patients with prearthritic hip disease. J Orthop Trauma 2018;32(Suppl 1):S30–4. https://doi.org/10.1097/BOT.0000000000001093.

[23] Nho SJ, Hu E, Cervantes JE. Editorial commentary: decreased hip ligament thickness in patients with dysplasia may contribute to hip instability, above and beyond associated acetabular under-coverage. Arthroscopy 2025;41(4):1000–1. https://doi.org/10.1016/j.arthro.2024.07.012.